Charge Transfer Reactions from I^- to Polar Protic Solvents Studied Using Ultrafast Extreme Ultraviolet Photoelectron Spectroscopy

Yo-ichi Yamamoto,[1] Yoshi-Ichi Suzuki,[2] and Toshinori Suzuki[1*]

[1]*Department of Chemistry, Graduate School of Science, Kyoto University, Kitashirakawa-Oiwakecho, Sakyo-Ku, Kyoto 606-8502, Japan*

[2]*School of Medical Technology, Health Sciences University of Hokkaido, 1757 Kanazawa, Tobetsucho, Ishikari, Hokkaido 061-0293, Japan*

* Correspondence to: *suzuki@kuchem.kyoto-u.ac.jp*

Abstract

Charge transfer reactions from I^- to solvent water, methanol, and ethanol were studied using extreme ultraviolet time-resolved photoelectron spectroscopy (EUV-TRPES). This technique eliminates spectral broadening, previously seen in UV-TRPES, caused by electron inelastic scattering in liquids, and enables clear observation of the temporal evolution of the spectral shape. The peak position, width, and intensity of the electron binding energy distribution indicate electron detachment and subsequent solvation and thermalization processes. Geminate recombination between detached electrons and iodine atoms is discussed using a diffusion equation and a global fitting analysis based on a kinetics model.

TOC graphics

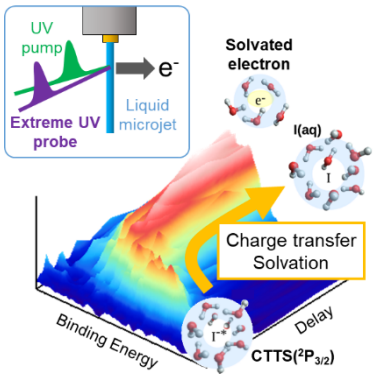

Elucidation of the static and dynamic influences of solvents on reactions is a central subject in solution chemistry. Since an electron has no rovibrational degrees of freedom, the evolution of the electronic state of an electron injected into a solvent is an excellent probe for studying solvation dynamics. The charge transfer to solvent (CTTS) reaction is an electron transfer process from a photoexcited solute to a solvent.[1] Iodide (I^-) ions in polar protic solvents exhibit metastable CTTS states, associated with the ^2P_J fine-structure levels of neutral I atoms, and these CTTS states undergo electron auto-detachment into the solvent.[2-4] The detachment is adiabatic at low photoexcitation energy, and produces a solvated electron (e^-_{solv}) in the vicinity of the iodine atom. Since HO bonds in the first solvation shell are orientated toward the central I^- ion,[5, 6] electron detachment induces solvation dynamics to newly stabilize the excess electron. The excess energy created by the solvation dynamics is dissipated into the surroundings by intermolecular energy transfer. A diffusive recombination reaction also occurs between e^-_{solv} and the iodine atom with a certain quantum yield.[7]

Since the CTTS states of iodide are easily accessible using UV radiation (190–260 nm), a plethora of studies have been reported using various spectroscopic methods such as transient absorption spectroscopy (TAS),[1, 8-13] time-resolved X-ray absorption spectroscopy,[14] and the fluorescence up-conversion method.[15] More recent studies were performed using time-resolved photoelectron spectroscopy (TRPES), which enables direct access to time-evolving electron binding energy (eBE) distributions.[16-20] TRPES with ultraviolet probe pulses (UV-TRPES) revealed a rapid increase in eBE due to reorganization of the solvation structure around the excess electrons. However, the eBE distribution exhibited distortion caused by electron inelastic scattering in the liquid and the energy dependence of the electron transmission efficiency through the gas-liquid interface.[21-23] In the present study, we employ TRPES with a femtosecond extreme UV (EUV; 47.1 nm, 27.9 eV) laser to address these technical problems and measure accurate eBE distributions.[24-30] The use of an EUV laser eliminates the distortions, because the elastic and rovibrationally inelastic scattering cross-sections are substantially reduced at high electron kinetic energy (eKE), and electron transmission through the interface also becomes energy-independent.[28] We investigate CTTS reactions from I^- to three polar protic solvents: liquid water, methanol (MeOH), and ethanol (EtOH), and compare their solvation dynamics.

Figure 1(a) shows EUV-TRPES results obtained for CTTS reactions from I^- to water, MeOH and EtOH. The vertical axis indicates the eBE, which is the difference between the probe photon energy and the observed eKE. In all cases, the eBE distribution rapidly shifts toward higher energy after photoexcitation owing to solvation of excess electrons. The timescale for these shifts is different among the solvents; it is much longer for alcohol than for water. For a quantitative analysis of the time scale, we extracted a non-equilibrium response, $S(t)$, defined as

$$S(t) = \frac{VBE(t) - VBE(\infty)}{VBE(0) - VBE(\infty)} \qquad (1)$$

in which *VBE* (vertical electron binding energy) corresponds to the peak of the eBE distribution at a given time delay. $VBE(\infty)$ values were fixed at 3.78, 3.39, and 3.25 eV for water, MeOH and EtOH, respectively, which were newly estimated in our laboratory. The results are shown in Figure 1(b); the black dots are experimental data and the solid lines are the results of least squares fitting using a bi-exponential function. The extracted time constants and preexponential factors are listed in Table 1. The short solvation time in water indicates that e^-_{solv} rapidly reaches an equilibrium state, while the slow dynamics in alcohol suggest that the structure and properties of e^-_{solv} in these solvents continuously vary over a picosecond timescale. The extracted time constants are in reasonable agreement with the values determined using UV-TRPES (Table 1).

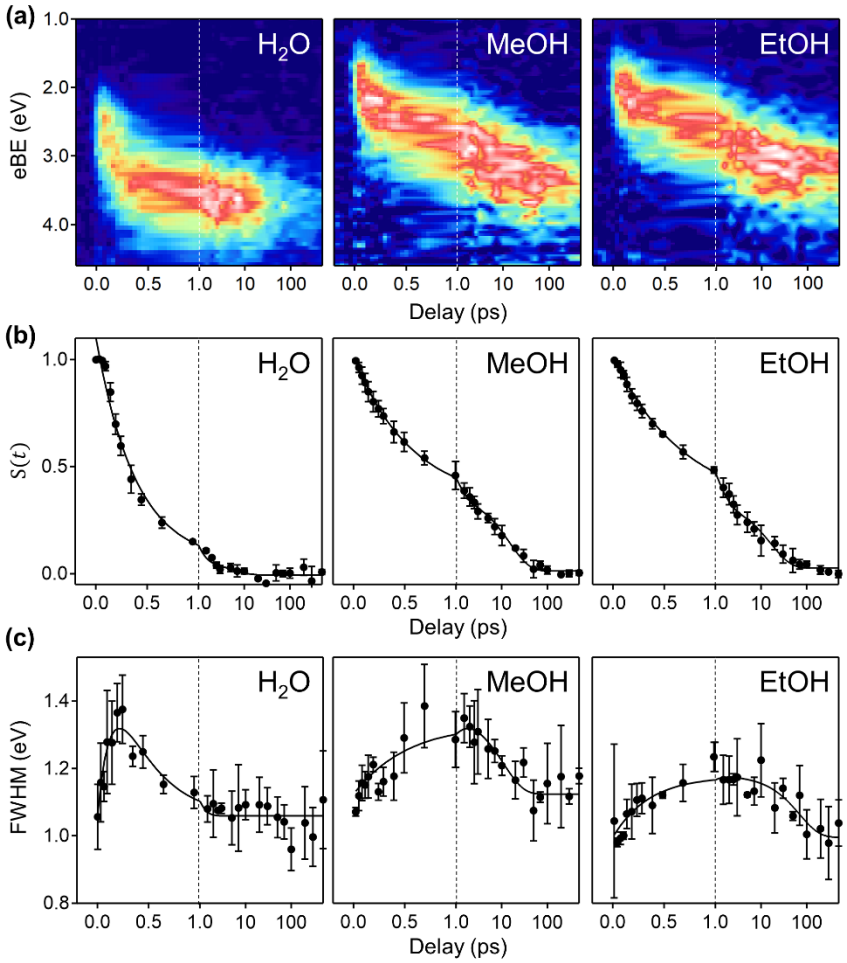

Figure 1. (a) EUV-TRPES data measured for CTTS reactions from I^- to water, MeOH and EtOH measured using the 225 nm (5.5 eV) pump pulses and 44.4 nm (27.9 eV) probe pulses. A coherent artifact at the time origin has been subtracted (See Section I in Supporting Information for details). (b) *S*(*t*) for *VBE* calculated from data shown in (a). (c) FWHM of the spectra shown in (a). The error bars are the standard deviations calculated from three independent measurements. The dots are the experimental data, and the solid

lines show the results of least-squares fitting. The horizontal axis is in linear scale up to 1 ps and logarithmic scale thereafter.

Table 1. Solvation time constants (ps) and preexponential factors

	Water	MeOH	EtOH
τ_1	0.38±0.04 0.4[a]	0.54±0.03 0.8[a]	0.68±0.05 1.1[a]
τ_2	5±7 2.7[a]	15±1 20[a]	16±3 45[a]
a_1	0.93±0.05 0.93[a]	0.64±0.01 0.63[a]	0.69±0.01 0.74[a]
a_2	0.07±0.05 0.07[a]	0.36±0.01 0.37[a]	0.31±0.01 0.26[a]

[a] UV-TRPES (Ref. [28])

On the other hand, EUV-TRPES revealed an interesting new feature. Figure 1(c) shows the eBE bandwidths observed for the three solvents. It is seen that the bandwidths vary with the pump-probe delay time in different manners for each solvent; this feature could be hardly examined with UV-TRPES owing to spectral broadening (comparison with the spectral retrieval analysis of UV-TRPES is presented in Section II, Supporting Information). In the case of water, the width rapidly increases with a time constant of 0.14±0.10 ps and decreases with a time constant of 0.34±0.23 ps. Previously, Messina et al. measured fluorescence from the CTTS state of I^- in an aqueous solution and found that fluorescence at the shortest wavelength of 310 nm decays in 60 fs, followed by a broad fluorescence in the visible region with the lifetime of about 200 fs.[15] Thus, the observed increase in the photoelectron bandwidth is likely occurring in the CTTS state prior to electron detachment, which is consistent with a broad visible emission spectrum measured previously. It is noted, however, while Messina et al. extracted a fast fluorescence component with a lifetime of 60 fs, the photoelectron spectrum exhibits continuous redshift and broadening, from which a fast component cannot be extracted clearly. In MeOH and EtOH, the bandwidth increases more slowly on a sub-picosecond time scale (0.59±0.24 and 0.36±0.12 ps, respectively) and decreases in 11 ± 6 ps for MeOH and 70 ± 30 ps for EtOH. As far as we notice, fluorescence up-conversion measurements have not been performed for alcohols; however, it is plausible that the increase in the bandwidth is correlated with the solvent response in the CTTS state. The decrease in the bandwidth is likely occurring after detachment of an excess electron owing to vibrational cooling. In both CTTS state and nascent state of e^-_{solv}, solvent response by translational and orientational ordering of solvent molecules reduces electrostatic energy and increases an internal energy of a system. Both of the dynamic structural rearrangements and increased vibrational energy will lead to spectral broadening of the system. Subsequent heat dissipation to the surroundings reduces the bandwidth. The considerably slower convergence of the EUV-TRPES spectral shape observed for alcohols is consistent with the results of a previous TAS study, where the absorption spectra of e^-_{solv} in alcohols converged to the thermal spectra in tens of picoseconds (see Figure 3).[10]

Also of particular interest are the EUV-induced photoelectron signal intensities presented in Figure 2 for (a) water, (b) MeOH, and (c) EtOH. In all cases, the observed intensities, plotted as black dots, gradually increase with increasing time delay on a picosecond timescale. It is noted that photodetachment from the CTTS state occurs on a sub-picosecond timescale,[8-12, 14-19, 31-38] and the number density of e^-_{solv} does not subsequently increase. Thus, the increase in the photoelectron signal intensity is ascribed to an increase in the photoabsorption cross-section at the EUV probe photon energy; this is presumably due to contraction of the electron wavefunction of e^-_{solv}. In order to extract and analyze the population of e^-_{solv} from the observed photoelectron signal intensity, we included a time-dependent photoabsorption cross-section in the following analysis.

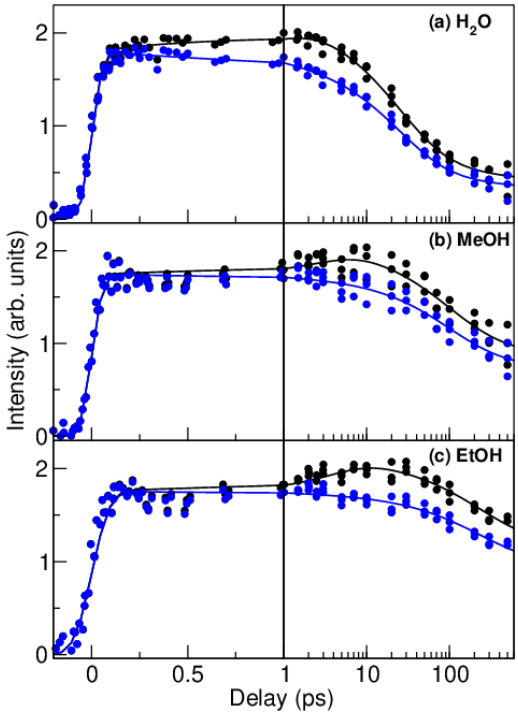

Figure 2. Total photoelectron intensity decay profiles measured using EUV-TRPES for NaI solutions in (a) water, (b) MeOH, and (c) EtOH. The black dots are the raw experimental data, and the blue dots are after calibration to account for variations in the EUV photoabsorption cross-section. The black solid line shows the results of least-squares fitting using a diffusion model. The horizontal axis is linear up to 1 ps and logarithmic afterwards. The pump and probe wavelengths were 225 and 44.4 nm, respectively.

The population decay for excess electrons in CTTS reactions is analyzed using the Smoluchowski diffusion equation. We employed the following equation,

$$\frac{\partial \psi(r,t)}{\partial t} = D' \frac{\partial}{\partial r} r^2 e^{-V(r)} \frac{\partial}{\partial r} r^{-2} e^{V(r)} \psi(r,t) \qquad (2)$$

where $\psi(r,t)$ is the net population of e^-_{solv} on a surface area of $4\pi r^2$, r is the distance of an electron from an iodine atom, D' is the mutual diffusion coefficient for the iodine-electron system, $D' = D(\mathrm{I}) + D(\mathrm{e}^-_{sol})$, and $V(r)$ is a potential of mean force. Previously, Iglev et al. assumed that an

electron is ejected at a distance of 0.61 nm from an iodine atom, and that geminate recombination immediately occurs at a contact radius, $r_{contact}$.[39] Kloepfer et al. assumed that geminate recombination at contact occurs with a rate constant κ_r (units of length/time),[8] and we also adopted this latter approach. We considered that an excess electron is ejected at a distance r_0 from the center of an iodine atom to create a time-dependent concentration of $r_a\{1 - exp(-t/\tau_a)\}$, where r_a and τ_a are the quantum yield and the effective time constant for electron detachment, respectively. The detached electron and iodine atom undergo diffusion in a potential,

$$V(r) = \Delta G\{1 - exp[-\beta(r - r_{min})]\}^2 - \Delta G \qquad (3)$$

in which ΔG and β are parameters describing the depth and width of the potential, respectively. In our simulation, r_0 and $r_{contact}$ were set to the potential minimum, r_{min}, β was 10 nm^{-1}, and r_a was assumed to be 1. These parameters were incorporated into the diffusion equation with a boundary condition of

$$\left(D' r^2 e^{-V(r)} \frac{\partial}{\partial r} r^{-2} e^{V(r)} \psi(r,t)\right)_{r=r_0} = \kappa_r \psi(r_0,t) - \frac{r_a}{\tau_a} P_{\mathrm{CTTS}}(t) \qquad (4)$$

where $P_{\mathrm{CTTS}}(t)$ is the number of transient species in the CTTS state per unit volume, i.e., $P_{CTTS}(t) = P_{\mathrm{CTTS}}(0)\exp(-\frac{t}{\tau_a})$. The photoelectron signal intensity is described as follows,

$$I(t) = \sigma(t)\{P_{\mathrm{CTTS}}(t) + P_e(t)\} \otimes g(t) \qquad (5)$$

where $P_e(t) = \int_{r_0}^{\infty} \psi(r,t)dr$ is the number of e^-_{solv} per unit volume. $g(t)$ is a Gaussian cross-correlation function between the pump and probe pulses. A time-dependent photoabsorption cross-section is introduced to express the aforementioned intensity increase on a picosecond time scale. The functional form is $\sigma(t) = C[1 + \sigma_\tau\{1 - exp(-t/\tau_\sigma)\}]$, where C, σ_τ, and τ_σ are fitting parameters. The blue dots in Figure 2 are the calibrated intensities for $\sigma(t)$. The best-fit parameters are summarized in Table 2.

When the TAS and EUV-TRPES data are compared as shown in Figure 3, the latter exhibit a faster intensity decay, indicating faster geminate recombination. This is ascribed to a lower sample temperature in EUV-TRPES than in TAS.[16] TRPES employed a liquid microjet injected into vacuum, and evaporative cooling caused the liquid temperature to be lower than the injection temperature. Slower diffusion at lower temperature reduces the electron escape probability, causing faster recombination. Iglev et al. performed a TAS study at three different temperatures of 298, 323, and 348 K, and found that ΔG can be regarded as temperature-independent in this range.[12] The temperature dependence of the recombination dynamics was ascribed to the strong variation of D', in addition to the small increase in β with increasing temperature.[12] We have tested this notion by simulating the decay curve at 298 K using the best-fit parameters determined at an estimated temperature of 278 K in EUV-TRPES and D'estimated from the viscosity of the solvent (Section III, Supporting Information). The simulated profile agrees reasonably well with the data at 298 K,

confirming the notion proposed by Iglev et al.[12] Similar results were obtained for MeOH and EtOH (Section IV, Supporting Information).

Table 2. Parameters obtained using diffusion equation

	TAS				EUV-TRPES		
	H_2O[a]	H_2O[b]	MeOH[c]	EtOH[c]	H_2O	MeOH	EtOH
T(K)	297	298	297	297	278[d]	260[d]	260[d]
$D' \times 10^5 (\mathrm{cm}^2/\mathrm{s})$	8	5.8	13.1	6.6	3.1[e]	1.7[e]	0.79[e]
$\Delta G/k_B T$	3.0	4.1	3.6	3.1	2.5	2.4	2.0
$\beta (\mathrm{nm}^{-1})$	11	6.8	10	10	10[e]	10[e]	10[e]
τ_a (ps)	0.2	0.22			0.39[e]	0.46[e]	0.68[e]
r_0(Å)	4.0	6.1	4.0	4.0	4.0[e]	4.0[e]	4.0[e]
σ_τ					0.25	0.19	0.22
τ_σ (ps)					1.1	3.0	4.1
κ_r (m/s)	5.2				4.3	0.93	0.37

[a] Reference [10]. D' is likely overestimated. See Ref. [[17]].
[b] Reference [12].
[c] Reference [31]. D' is likely overestimated.
[d] The temperatures of liquid microjets were estimated based on the Raman thermometry by Wilson *et al.* [40].
[e] Fixed

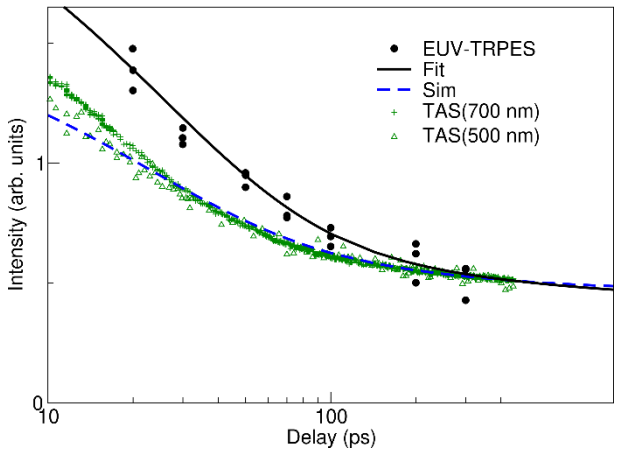

Figure. 3 EUV-TRPES data (black dots) obtained for CTTS reaction in water at 278 K using the 225 nm (5.5 eV) pump pulses and 44.4 nm (27.9 eV) probe pulses, and least-squares fitting (black solid line) using diffusion equation with $D' = 3.1 \times 10^{-5}$ cm^2/s. The blue dashed line is a numerical prediction for EUV-TRPES at 297 K ($D' = 5.7 \times 10^{-5}$ cm^2/s). TAS data at 297 K[10] are indicated by + (700 nm) and Δ (500 nm). Intensities are normalized at 400 ps.

An alternative method generally employed for the analysis of TAS and TRPES results is global fitting. While the aforementioned diffusion analysis only considers the signal intensity, global fitting simulates both the spectral evolution and signal intensity. Figure 4(a) depicts the kinetic scheme employed for our analysis. This model assumes four kinetic steps involving (i) formation of the CTTS state by photoexcitation, (ii) relaxation to a contact pair (CP), (iii) further separation to

form a solvent-separated state (SS), and (iv) separation into a free e^-_{solv} and an iodine atom. Geminate recombination is assumed to be possible from all transient states in this model, although it will be shown later that recombination is important only from the SS state. The analytical solutions for this kinetic model are as follows:

$$[CTTS] = e^{-t/\tau_a} \tag{6}$$

$$[CP] = r_a\tau_b\left(\frac{e^{-t/\tau_a}}{\tau_{ab}} + \frac{e^{-t/\tau_b}}{\tau_{ba}}\right) \tag{7}$$

$$[SS] = r_a r_b \tau_c\left(\frac{\tau_a e^{-t/\tau_a}}{\tau_{ab}\tau_{ac}} + \frac{\tau_b e^{-t/\tau_b}}{\tau_{ba}\tau_{bc}} + \frac{\tau_c e^{-t/\tau_c}}{\tau_{ca}\tau_{cb}}\right) \tag{8}$$

$$[SE] = r_a r_b r_c \tau_d\left(\frac{\tau_a^2 e^{-t/\tau_a}}{\tau_{ab}\tau_{ac}\tau_{ad}} + \frac{\tau_b^2 e^{-t/\tau_b}}{\tau_{ba}\tau_{bc}\tau_{bd}} + \frac{\tau_c^2 e^{-t/\tau_c}}{\tau_{ca}\tau_{cb}\tau_{cd}} + \frac{\tau_d^2 e^{-t/\tau_d}}{\tau_{da}\tau_{db}\tau_{dc}}\right) \tag{9}$$

$$I(t) = \sigma(t)(c_{ak}[CTTS] + c_{bk}[CP] + c_{ck}[SS] + c_{dk}[SE]) \otimes g(t) \tag{10}$$

where $\tau_x^{-1} = \tau_{x1}^{-1} + \tau_{x2}^{-1}(x = a, b, c, d)$, $\tau_{xy} = \tau_x - \tau_y\ (x, y = a, b, c, d)$, and $r_x = \tau_x\tau_{x1}^{-1}(x = a, b, c)$ are the branching ratios for each step, $g(t)$ is a Gaussian cross-correlation function for the laser pulses, $c_{xk}\ (x = a, b, c, d)$ is an expansion coefficient, and k is an index for equally spaced *eBE* bins. The parameters for $\sigma(t)$ were fixed to those determined by the diffusion model and assumed to be common for all transient states.

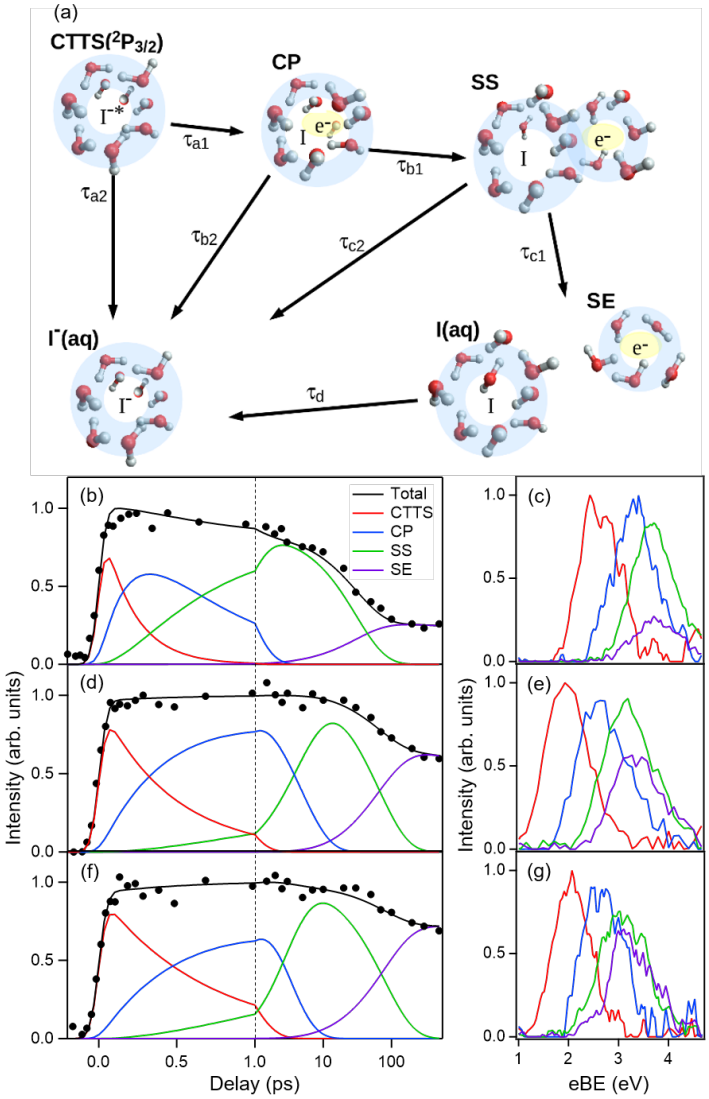

Figure 4. Kinetic analysis of CTTS reaction. (a) Illustration of charge transfer reaction and kinetics scheme. CTTS: charge transfer to solvent state, CP: contact pair, SS: solvent-separated state, SE: e^-_{solv}. (b), (d), (f) Time evolution of transient species reproduced by least-squares global fitting for water, MeOH, and EtOH, respectively. Black dots are the signal intensities calibrated for variation of the absorption cross-sections. (c), (e), (g) Extracted spectra associated with each transient for water, MeOH, and EtOH, respectively. The horizontal axis is linear up to 1 ps and logarithmic afterwards.

Figures 4(b)–(g) show the results of global fitting (Section V, Supporting Information), assuming a time-independent spectrum associated with each transient state. The determined time constants are listed in Table 3. The results indicate that the overall yield of e^-_{solv} is 0.28, 0.62, and 0.75 for water, MeOH and EtOH, respectively. The kinetic model expresses electron escape by τ_{c1} and the escape yield in the last step by r_c=τ_c/τ_{c1}. Our r_c value (0.32) for water is comparable to the value of 0.32 estimated by Kloepfer et al. for a bulk solution,[9] and the value of 0.30 estimated by Nowakowski et al. for a gas-liquid interface.[33] The overall long-period signal decay time of 31 ps is

comparable to the values of 23 ps estimated by Kloepfer et al.[9] and 16 ps estimated by Nowakowski et al.[33]

For least-squares fitting using the kinetic model, the quality of the fit is always improved by assuming a larger number of transient states; here we assumed the minimal number of intermediate states (CP and SS). However, as seen in Figures 1(a), 4(c), 4(e), and 4(g) the spectra exhibit a continuous energy shift but no large variation in shape, so that it is difficult to categorize the continuously evolving state into only two species of CP and SS.

Table 3. Kinetic time constants (ps) and branching ratios determined for NaI solutions by EUV-TRPES

	H_2O	MeOH	EtOH
τ_a	0.20[a]	0.46[a]	0.68[a]
τ_b	0.57±0.04	4.6±0.4	2.6±0.2
τ_c	31±1	65±8	80±10
τ_d	1×10^{8}[b]	1×10^{8}[b]	1×10^{8}[b]
τ_{a1}	0.20	0.46	0.68
τ_{a2}	-	17.0±0.3	-
τ_{b1}	0.65±0.04	4.6±0.4	2.8±0.2
τ_{b2}	4.3±0.3	-	40±4
τ_{c1}	95±5	101±12	105±14
τ_{c2}	45±2	180±20	320±40
r_a	1.01±0.02	0.97±0.02	1.07±0.02
r_b	0.87±0.01	1.00±0.02	0.94±0.02
r_c	0.32±0.01	0.64±0.01	0.75±0.01

a Fixed.

b These values are too large to determine accurately in our measurements.

In conclusion, EUV-TRPES enabled accurate measurements of the temporal evolution of eBE distributions free from the influence of electron inelastic scattering in the liquid. The photoelectron signal intensity measured for water, methanol, and ethanol solution exhibited an initial growth. This indicates that the quantum yield for electron detachment from the CTTS state of I^- is essentially unity in all cases, and that the optical absorption cross-section for the transient species grows with the progressive formation of a stable solvation shell for the excess electron and the associated contraction of the electron wavefunction for e^-_{solv}. The eBE bandwidth also revealed an initial growth in all solvents, indicating the growth of structural inhomogeneity due to formation of a new solvation shell and vibrational heating associated with electronic relaxation. The analysis using a diffusion equation suggests the depth of the mean force potentials to be 2.5, 2.4, and 2.0 times k_BT for water, methanol, and ethanol, respectively. The difference in geminate recombination between 273 and 298 K is reasonably well explained by considering only the temperature dependence of mutual diffusion coefficients.

Experimental Methods

A continuous liquid microjet of 0.2 M NaI solution was generated by discharging a solution through a fused silica capillary with an inner diameter of 25 μm (water) or 15 μm (alcohol) into a photoionization chamber. The flow rates were 0.5 and 0.2 mL/min for water and alcohol, respectively. The details of our vacuum chambers and the magnetic bottle time-of-flight photoelectron spectrometer (MBTOF) have been described elsewhere.[41] A 10-kHz Ti:sapphire regenerative amplifier (800 nm (ω), 0.7 mJ, 35 fs) was used to generate UV pump and EUV probe pulses. The UV (225 nm, 5.5 eV) pump pulses were generated with an optical parametric amplifier and focused on a liquid microjet using an Al concave mirror (r = 2000 mm). The UV pulse energies at the sample were less than 150, 60 and 30 nJ for water, MeOH and EtOH solutions, respectively. The EUV probe pulses were generated by focusing the second harmonic (2ω) of the Ti:sapphire laser radiation into an Ar gas cell, and the multiple harmonics thus generated were dispersed using a time-preserving monochromator to obtain a single 18ω (47.1 nm, 27.9 eV) harmonic.[42] The energy-selected EUV pulses were focused on a liquid microjet using a toroidal mirror. The eKE distribution was measured using a 1.3-m-long MBTOF analyzer with an energy resolution of 50 meV and an A/D converter. The absolute eKE value was energy-calibrated using the vertical ionization energy for the solvent: 11.3 (water), 9.70 (MeOH) and 9.52 eV (EtOH).[43, 44] The cross-correlation time between the UV pump and EUV probe pulses was measured to be 90-100 fs using coherent two-photon ionization of the solvents. The penetration depth of the UV and EUV radiation in the solutions is more than 1 μm, while the probing depth of EUV-TRPES is about 1 nm owing to the limited escape depth for electrons from the liquid.

Acknowledgment

This work was supported by the JSPS KAKENHI Grant Number 21H04970.

Supporting Information Available:

Estimation of cross-correlation time between UV pump and EUV probe pulses, comparison of time evolution of spectral width of EUV-TRPES with those of the spectral retrieval analysis of UV-TRPES, estimation of the temperature dependence of diffusion coefficients, temperature dependence in geminate recombination in alcohol, and the results of global fitting analysis of EUV -TRPES data.

References

(1) Chen, X. Y.; Bradforth, S. E. The Ultrafast Dynamics of Photodetachment. *Annu. Rev. Phys. Chem.* **2008**, *59*, 203-231.

(2) Sheu, W. S.; Rossky, P. J. Dynamics of Electron Photodetachment from an Aqueous Halide Ion. *Chem. Phys. Lett.* **1993**, *213*, 233-238.

(3) Sheu, W. S.; Rossky, P. J. Charge-Transfer-to-Solvent Spectra of an Aqueous Halide Revisited via Computer-Simulation. *J. Am. Chem. Soc.* **1993**, *115*, 7729-7735.

(4) Sheu, W. S.; Rossky, P. J. Electronic and Solvent Relaxation Dynamics of a Photoexcited Aqueous Halide. *J. Phys. Chem.* **1996**, *100*, 1295-1302.

(5) Bradforth, S. E.; Jungwirth, P. Excited States of Iodide Anions in Water: A Comparison of the Electronic Structure in Clusters and in Bulk Solution. *J. Phys. Chem. A* **2002**, *106*, 1286-1298.

(6) Bhattacharyya, D.; Mizuno, H.; Rizzuto, A. M.; Zhang, Y. Y.; Saykally, R. J.; Bradforth, S. E. New Insights into the Charge-Transfer-to-Solvent Spectrum of Aqueous Iodide: Surface Versus Bulk. *J. Phys. Chem. Lett.* **2020**, *11*, 1656-1661.

(7) Staib, A.; Borgis, D. Reaction Pathways in the Photodetachment of an Electron from Aqueous Chloride: A Quantum Molecular Dynamics Study. *J. Chem. Phys.* **1996**, *104*, 9027-9039.

(8) Kloepfer, J. A.; Vilchiz, V. H.; Lenchenkov, V. A.; Germaine, A. C.; Bradforth, S. E. The Ejection Distribution of Solvated Electrons Generated by the One-Photon Photodetachment of Aqueous I^- and Two-Photon Ionization of the Solvent. *J. Chem. Phys.* **2000**, *113*, 6288-6307.

(9) Kloepfer, J. A.; Vilchiz, V. H.; Lenchenkov, V. A.; Chen, X. Y.; Bradforth, S. E. Time-Resolved Scavenging and Recombination Dynamics from I : e^- Caged Pairs. *J. Chem. Phys.* **2002**, *117*, 766-778.

(10) Vilchiz, V. H.; Chen, X. Y.; Kloepfer, J. A.; Bradforth, S. E. Solvent Effects on Geminate Recombination Dynamics after Photodetachment. *Radiat. Phys. Chem.* **2005**, *72*, 159-167.

(11) Moskun, A. C.; Bradforth, S. E.; Thogersen, J.; Keiding, S. Absence of a Signature of Aqueous I($P^2_{1/2}$) after 200-nm Photodetachment of I^-(aq). *J. Phys. Chem. A* **2006**, *110*, 10947-10955.

(12) Iglev, H.; Trifonov, A.; Thaller, A.; Buchvarov, I.; Fiebig, T.; Laubereau, A. Photoionization Dynamics of an Aqueous Iodide Solution: The Temperature Dependence. *Chem. Phys. Lett.* **2005**, *403*, 198-204.

(13) Fischer, M. K.; Laubereau, A.; Iglev, H. Femtosecond Electron Detachment of Aqueous Bromide Studied by Two and Three Pulse Spectroscopy. *Phys. Chem. Chem. Phys.* **2009**, *11*, 10939-10944.

(14) Pham, V. T.; Gawelda, W.; Zaushitsyn, Y.; Kaiser, M.; Grolimund, D.; Johnson, S. L.; Abela, R.; Bressler, C.; Chergui, M. Observation of the Solvent Shell Reorganization around Photoexcited Atomic Solutes by Picosecond X-Ray Absorption Spectroscopy. *J. Am. Chem. Soc.* **2007**, *129*, 1530-1531.

(15) Messina, F.; Bram, O.; Cannizzo, A.; Chergui, M. Real-Time Observation of the Charge Transfer to Solvent Dynamics. *Nat. Commun.* **2013**, *4*, 2119.

(16) Suzuki, Y. I.; Shen, H.; Tang, Y.; Kurahashi, N.; Sekiguchi, K.; Mizuno, T.; Suzuki, T. Isotope Effect on Ultrafast Charge-Transfer-to-Solvent Reaction from I^- to Water in Aqueous NaI Solution. *Chem. Sci.* **2011**, *2*, 1094-1102.

(17) Okuyama, H.; Suzuki, Y. I.; Karashima, S.; Suzuki, T. Charge-Transfer-to-Solvent Reactions from I^- to

Water, Methanol, and Ethanol Studied by Time-Resolved Photoelectron Spectroscopy of Liquids. *J. Chem. Phys.* **2016**, *145*, 074502.
(18) Lubcke, A.; Buchner, F.; Heine, N.; Hertel, I. V.; Schultz, T. Time-Resolved Photoelectron Spectroscopy of Solvated Electrons in Aqueous NaI Solution. *Phys. Chem. Chem. Phys.* **2010**, *12*, 14629-14634.
(19) Elkins, M. H.; Williams, H. L.; Neumark, D. M. Dynamics of Electron Solvation in Methanol: Excited State Relaxation and Generation by Charge-Transfer-to-Solvent. *J. Chem. Phys.* **2015**, *142*, 234501.
(20) Suzuki, T. Ultrafast Photoelectron Spectroscopy of Aqueous Solutions. *J. Chem. Phys.* **2019**, *151*, 090901.
(21) Yamamoto, Y.; Karashima, S.; Adachi, S.; Suzuki, T. Wavelength Dependence of UV Photoemission from Solvated Electrons in Bulk Water, Methanol, and Ethanol. *J. Phys. Chem. A* **2016**, *120*, 1153-1159.
(22) Luckhaus, D.; Yamamoto, Y. I.; Suzuki, T.; Signorell, R. Genuine Binding Energy of the Hydrated Electron. *Sci. Adv.* **2017**, *3*, e1603224.
(23) Scholz, M. S.; Fortune, W. G.; Tau, O.; Fielding, H. H. Accurate Vertical Ionization Energy of Water and Retrieval of True Ultraviolet Photoelectron Spectra of Aqueous Solutions. *J. Phys. Chem. Lett.* **2022**, *13*, 6889-6895.
(24) Siefermann, K. R.; Liu, Y. X.; Lugovoy, E.; Link, O.; Faubel, M.; Buck, U.; Winter, B.; Abel, B. Binding Energies, Lifetimes and Implications of Bulk and Interface Solvated Electrons in Water. *Nat. Chem.* **2010**, *2*, 274-279.
(25) Ojeda, J.; Arrell, C. A.; Longetti, L.; Chergui, M.; Helbing, J. Charge-Transfer and Impulsive Electronic-to-Vibrational Energy Conversion in Ferricyanide: Ultrafast Photoelectron and Transient Infrared Studies. *Phys. Chem. Chem. Phys.* **2017**, *19*, 17052-17062.
(26) Engel, N.; Bokarev, S. I.; Moguilevski, A.; Raheem, A. A.; Al-Obaidi, R.; Mohle, T.; Grell, G.; Siefermann, K. R.; Abel, B.; Aziz, S. G. Kuhn, O.; Borgwardt, M.; Kiyan, I. Y.; Aziz, E. F. Light-Induced Relaxation Dynamics of the Ferricyanide Ion Revisited by Ultrafast XUV Photoelectron Spectroscopy. *Phys. Chem. Chem. Phys.* **2017**, *19*, 14248-14255.
(27) Hummert, J.; Reitsma, G.; Mayer, N.; Ikonnikov, E.; Eckstein, M.; Kornilov, O. Femtosecond Extreme Ultraviolet Photoelectron Spectroscopy of Organic Molecules in Aqueous Solution. *J. Phys. Chem. Lett.* **2018**, *9*, 6649-6655.
(28) Nishitani, J.; Yamamoto, Y.; West, C. W.; Karashima, S.; Suzuki, T. Binding Energy of Solvated Electrons and Retrieval of True UV Photoelectron Spectra of Liquids. *Sci. Adv.* **2019**, *5*, aaw6896.
(29) Longetti, L.; Barillot, T. R.; Puppin, M.; Ojeda, J.; Poletto, L.; van Mourik, F.; Arrell, C. A.; Chergui, M. Ultrafast Photoelectron Spectroscopy of Photoexcited Aqueous Ferrioxalate. *Phys. Chem. Chem. Phys.* **2021**, *23*, 25308-25316.
(30) Wang, C.; Waters, M. D. J.; Zhang, P.; Suchan, J.; Svoboda, V.; Luu, T. T.; Perry, C.; Yin, Z.; Slavicek, P.; Worner, H. J. Different Time Scales During Ultrafast Stilbene Isomerization in the Gas and Liquid Phases Revealed Using Time-Resolved Photoelectron Spectroscopy. *Nat. Chem.* **2022**, *14*, 1126–1132.
(31) Vilchiz, V. H.; Kloepfer, J. A.; Germaine, A. C.; Lenchenkov, V. A.; Bradforth, S. E. Map for the Relaxation Dynamics of Hot Photoelectrons Injected into Liquid Water via Anion Threshold Photodetachment and above Threshold Solvent Ionization. *J. Phys. Chem. A* **2001**, *105*, 1711-1723.

(32) Iwata, A.; Nakashima, N.; Kusaba, M.; Izawa, Y.; Yamanaka, C. Quantum Yields of Hydrated Electrons by UV Laser Irradiation. *Chem. Phys. Lett.* **1993**, *207*, 137-142.
(33) Nowakowski, P. J.; Woods, D. A.; Verlet, J. R. R. Charge Transfer to Solvent Dynamics at the Ambient Water/Air Interface. *J. Phys. Chem. Lett.* **2016**, *7*, 4079-4085.
(34) Shen, H. A.; Kurahashi, N.; Horio, T.; Sekiguchi, K.; Suzuki, T. Direct Measurement of Vertical Electron Binding Energies of Solvated Electrons in Methanol and Ethanol. *Chem. Lett.* **2010**, *39*, 668-670.
(35) Tang, Y.; Shen, H.; Sekiguchi, K.; Kurahashi, N.; Mizuno, T.; Suzuki, Y. I.; Suzuki, T. Direct Measurement of Vertical Binding Energy of a Hydrated Electron. *Phys. Chem. Chem. Phys.* **2010**, *12*, 3653-3655.
(36) Tang, Y.; Suzuki, Y. I.; Shen, H.; Sekiguchi, K.; Kurahashi, N.; Nishizawa, K.; Zuo, P.; Suzuki, T. Time-Resolved Photoelectron Spectroscopy of Bulk Liquids at Ultra-Low Kinetic Energy. *Chem. Phys. Lett.* **2010**, *494*, 111-116.
(37) Shreve, A. T.; Yen, T. A.; Neumark, D. M. Photoelectron Spectroscopy of Hydrated Electrons. *Chem. Phys. Lett.* **2010**, *493*, 216-219.
(38) Shreve, A. T.; Elkins, M. H.; Neumark, D. M. Photoelectron Spectroscopy of Solvated Electrons in Alcohol and Acetonitrile Microjets. *Chem. Sci.* **2013**, *4*, 1633-1639.
(39) Iglev, H.; Laenen, R.; Laubereau, A. Femtosecond Dynamics of Electron Photodetachment of the Fluoride Anion in Liquid Water. *Chem. Phys. Lett.* **2004**, *389*, 427-432.
(40) Wilson, K. R.; Rude, B. S.; Smith, J.; Cappa, C.; Co, D. T.; Schaller, R. D.; Larsson, M.; Catalano, T.; Saykally, R. J. Investigation of Volatile Liquid Surfaces by Synchrotron X-Ray Spectroscopy of Liquid Microjets. *Rev. Sci. Instrum.* **2004**, *75*, 725-736.
(41) Kurahashi, N.; Thurmer, S.; Liu, S. Y.; Yamamoto, Y. I.; Karashima, S.; Bhattacharya, A.; Ogi, Y.; Horio, T.; Suzuki, T. Design and Characterization of a Magnetic Bottle Electron Spectrometer for Time-Resolved Extreme UV and X-Ray Photoemission Spectroscopy of Liquid Microjets. *Struct. Dynam.* **2021**, *8*, 034303.
(42) Frassetto, F.; Cacho, C.; Froud, C. A.; Turcu, I. C. E.; Villoresi, P.; Bryan, W. A.; Springate, E.; Poletto, L. Single-Grating Monochromator for Extreme-Ultraviolet Ultrashort Pulses. *Opt. Express* **2011**, *19*, 19169-19181.
(43) Kurahashi, N.; Karashima, S.; Tang, Y.; Horio, T.; Abulimiti, B.; Suzuki, Y. I.; Ogi, Y.; Oura, M.; Suzuki, T. Photoelectron Spectroscopy of Aqueous Solutions: Streaming Potentials of NaX (X = Cl, Br, and I) Solutions and Electron Binding Energies of Liquid Water and X^-. *J. Chem. Phys.* **2014**, *140*, 174506.
(44) Thuermer, S.; Shinno, T.; Suzuki, T. Valence Photoelectron Spectra of Liquid Methanol and Ethanol Measured Using He II Radiation. *J. Phys. Chem. A* **2021**, *125*, 2492-2503.

Supporting Information

Charge Transfer Reactions from I^- to Polar Protic Solvents Studied Using Ultrafast Extreme Ultraviolet Photoelectron Spectroscopy

Yo-ichi Yamamoto,[1] Yoshi-Ichi Suzuki,[2] and Toshinori Suzuki[1*]

[1]*Department of Chemistry, Graduate School of Science, Kyoto University, Kitashirakawa-Oiwakecho, Sakyo-Ku, Kyoto 606-8502, Japan*

[2]*School of Medical Technology, Health Sciences University of Hokkaido, 1757 Kanazawa, Tobetsucho, Ishikari, Hokkaido 061-0293, Japan*

I. Estimation of cross-correlation time between UV pump and EUV probe pulses

The spectra observed for sample solutions exhibit a strong short-lived signal in the electron binding energy (eBE) region above 5 eV due to non-resonant (1+1') ionization of solvent induced by the UV pump and extreme UV (EUV) probe pulses. The Figure S1(a) shows an example. The coherent artifact is well separated from the signal of the excited state of iodides and solvated electrons (e^-_{solv}) appearing in the eBE region bellow 4 eV. The integrated intensity of the coherent artifact is well expressed by a Gaussian function centered at the time origin as shown in Figure S1(b), and the FWHM provides the cross-correlation time of 90-100 fs. The coherent artifact has already been subtracted in Figures 1(a), (b), and (c).

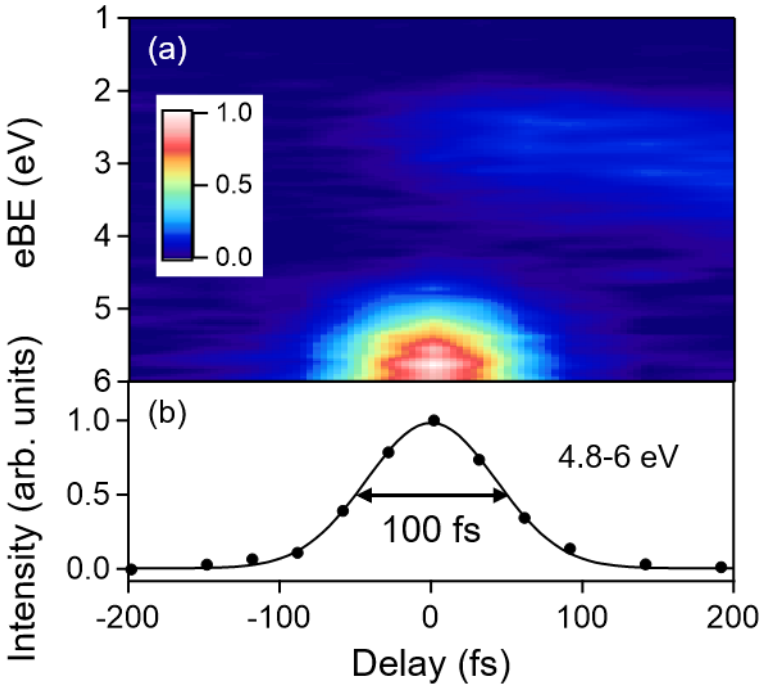

Figure S1. (a) Photoelectron spectra measured for aqueous 0.2 M NaI solution before subtraction of a coherent artifact. (b) Integrated intensity over eBE region of 4.8-6 eV (dots) and the result of Gaussian fitting (solid line).

II. Comparison between EUV-TRPES and Spectral Retrieval Analysis of UV-TRPES

We have recently developed a spectral retrieval (SR) method that performs a linear transformation of UV time-resolved Photoelectron spectroscopy (UV-TRPES) data to recover sharp photoelectron spectra[1]. Figure S2 compares the observed bandwidths in EUV-TRPES and those retrieved from UV-TRPES data. One can see that crude features are successfully captured in the SR/UV-TRPES, while the remaining discrepancy indicates the current limit in the accuracy of the SR analysis.

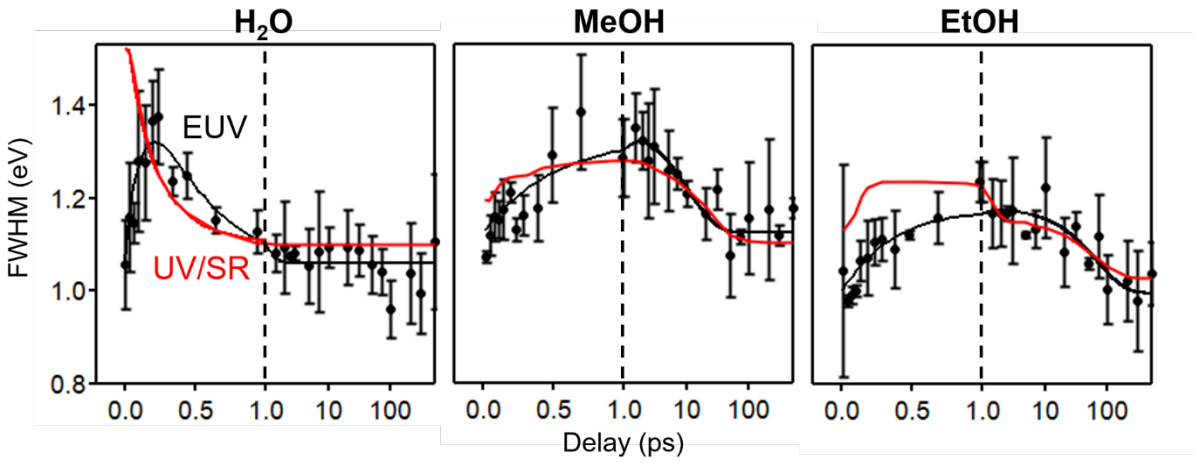

Figure S2. Comparison of the temporal evolution of band width between EUV-TRPES (black) and Spectral Retrieval Analysis of UV-TRPES (red). The horizontal axis is linear up to 1 ps and logarithmic afterwards.

III. Diffusion coefficient

The diffusion coefficient (D) depends on the solute (X), solvent (Y) and temperature (T), and it is expressed as $D(X, Y, T)$. Experimental values for D are often not available in the literature, so we estimated them using the Stokes-Einstein relation, $D = \frac{k_B T}{6\pi\eta a}$, where k_B is the Boltzmann constant, η is the viscosity, and a is the radius of the solute. It should be noted that the radius a for an electron depends on the solvent due to the solvation-shell structure. The value of η is strongly dependent on Y and T, and is expressed by $\eta = \eta(Y, T)$. For simplicity, when the temperature dependence of the diffusion coefficient was unknown, only the temperature dependence of the viscosity of the solvent was considered. This seems a reasonable assumption; the reported diffusion coefficient for an electron in water is well reproduced by the temperature dependence of viscosity (Table S1), especially in the range of 278-298 K. To the best of our knowledge, there is no experimentally determined diffusion coefficient for iodine atoms in water. Hence, the mutual diffusion coefficient D' in liquid water is estimated by

$$D' = D_{exp}(e^-, \mathrm{H_2O}, T) + D_{sim}(\mathrm{I}, \mathrm{H_2O}, 298.15\ \mathrm{K})\frac{\eta(\mathrm{H_2O}, 298.15\ \mathrm{K})}{\eta(\mathrm{H_2O}, T)} \quad \text{(S1)},$$

where D_{exp} and D_{sim} are the experimentally determined diffusion coefficient for e^-_{solv},[2] and a coefficient calculated for iodine atoms at 298.15 K using molecular dynamics simulations, respectively.[3] Since the diffusion coefficient for iodine atoms in alcohol is also unknown, we approximated it using the corresponding value in water as follows,

$$D' = D_{exp}(e^-, \mathrm{solvent}, 298\ \mathrm{K})\frac{\eta(\mathrm{solvent}, 298\ \mathrm{K})}{\eta(\mathrm{solvent}, T)} + D_{sim}(\mathrm{I}, \mathrm{H_2O}, 298.15\ \mathrm{K})\frac{\eta(\mathrm{solvent}, 298.15\ \mathrm{K})}{\eta(\mathrm{solvent}, T)} \quad \text{(S2)},$$

where D_{exp} is an experimentally determined diffusion coefficient.[4] The mutual diffusion coefficient for methanol is smaller than that for water due to the first term, even though methanol is less viscous than

water. We used the temperature-dependent viscosity reported by Xiang et al.[5] and Gonçalves et al.[6] for MeOH and EtOH, respectively.

Table S1. Temperature dependence of relative diffusion coefficient and viscosity in liquid water

T(K)	278	298	323	348	
$D'(T)/D'(298\ \mathrm{K})$		1	1.64	2.33	Ref. [7]
$D_e\text{-}(T)/D_e\text{-}\ (298\ K)$	0.51	1	1.86	3.18	Ref. [8]
$\eta(298\ \mathrm{K})/\ \eta(T)$	0.59	1	1.63	2.35	

IV. Temperature dependence of geminate recombination in MeOH and EtOH

Iglev et al.[7] claimed that the temperature dependence of the geminate recombination reaction can be attributed to the temperature dependence of the mutual diffusion coefficient. In the main text, we showed that the rate of geminate recombination in water at room temperature can be rather well reproduced by fixing the parameters obtained from EUV-TRPES data for e^-_{solv} and considering only the temperature dependence of the mutual diffusion coefficient. The decay curve for the population of e^-_{solv} at room temperature was reasonably well reproduced. As shown in Figures S3 and S4, the rate of geminate recombination can be reasonably well reproduced also for alcohol by fixing various parameters obtained by EUV-TRPES and considering the temperature dependence of the mutual diffusion coefficient. However, the following points should be considered. Firstly, the sample temperature in EUV-TRPES is an estimate, and not obtained by spectroscopic measurement. Secondly, energy relaxation in the charge transfer to solvent reaction and subsequent cooling may vary the local temperature slightly. As shown in Figures S3 and S4, the decay curves for the transient absorption spectroscopy (TAS) signal observed at wavelengths of 700 and 500 nm do not match in the time range up to about 100 ps. Thus, a discussion based on the temperature of the bulk solution is only expected to be valid for long delay times.

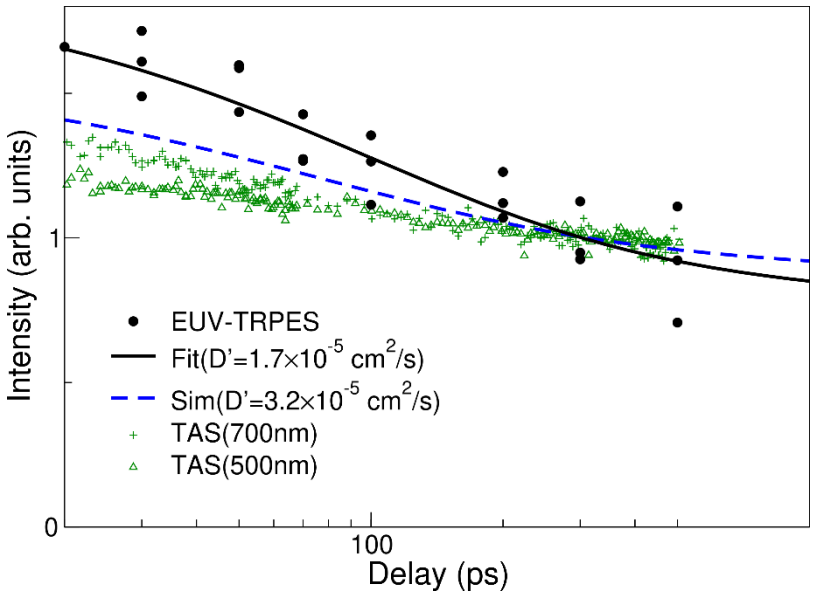

Figure S3. Least-squares fit of EUV-TRPES results (black) for e_{MeOH}^- at 260 K and TAS at 297 K.[9] The crosses and open triangles are experimental data for different absorption wavelengths. The dashed line is a simulation for EUV-TRPES at 297 K. Intensities are normalized at 300 ps. The difference between the TRPES and TAS results is primarily due to the difference in temperature.

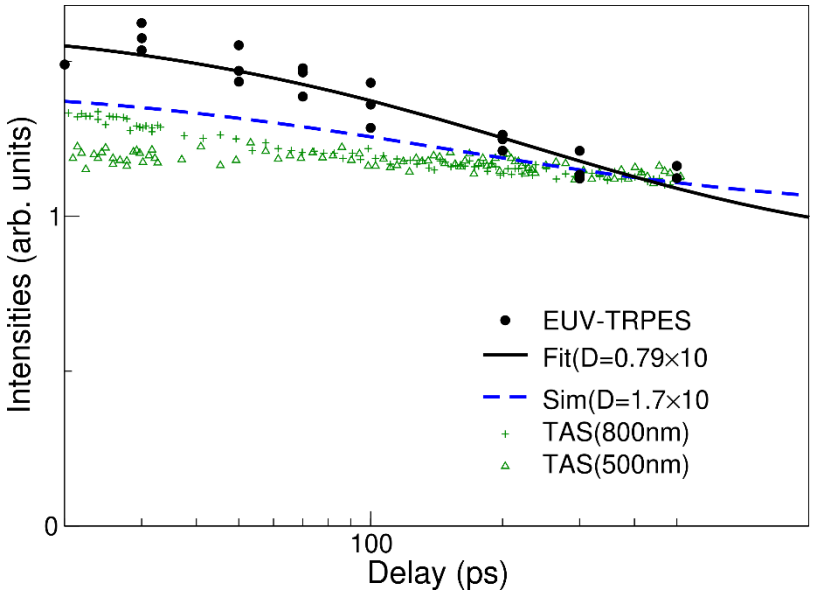

Figure S4. Least-squares fit of EUV-TRPES results (black) for e_{EtOH}^- at 260 K and TAS at 297 K.[9] The crosses and open triangles are experimental data for different absorption wavelengths. The dashed line is a simulation for EUV-TRPES at 297 K. Intensities are normalized at 400 ps. The difference between the TRPES and TAS results is primarily due to the difference in temperature.

V. Global fitting analysis of EUV-TRPES data

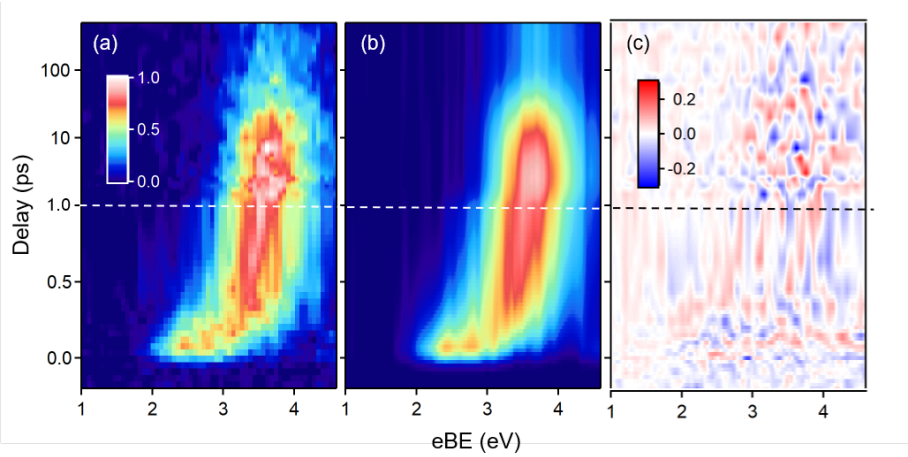

Figure S5. Global fitting results for EUV-TRPES data measured for aqueous 0.2 M NaI solution. (a) observed photoemission spectra. (b) spectra reproduced using kinetic model shown in Fig. 4(a). (c) Residuals of fitting process. The vertical axis is linear up to 1 ps and logarithmic afterwards.

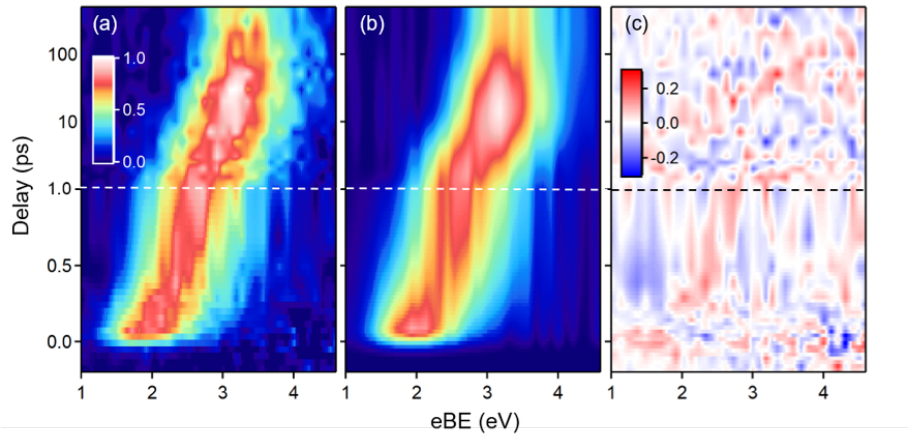

Figure S6. Global fitting results for EUV-TRPES data measured for 0.2 M NaI MeOH solution. (a) observed photoemission spectra. (b) reproduced spectra using kinetic model shown in Fig. 4(a). (c) Residuals of fitting process. The vertical axis is linear up to 1 ps and logarithmic afterwards.

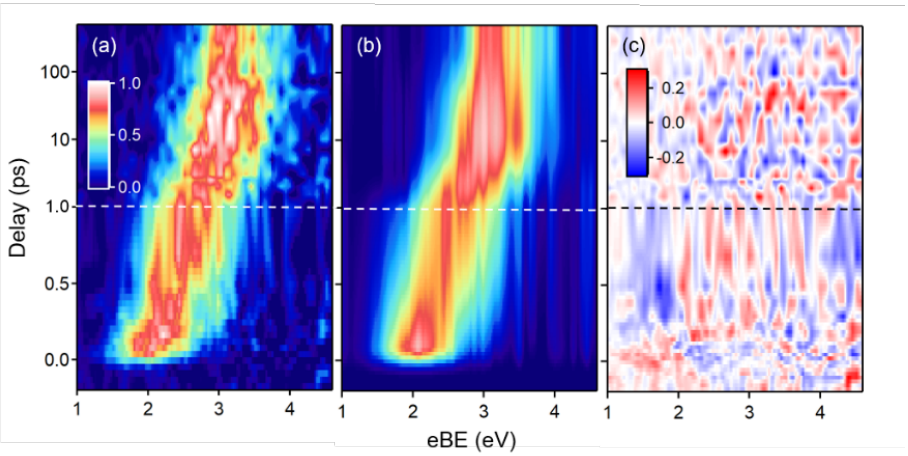

Figure S7. Global fitting results for EUV-TRPES data measured for 0.2 M NaI EtOH solution. (a) observed photoemission spectra. (b) reproduced spectra using kinetic model shown in Fig. 4(a). (c) Residuals of fitting process. The vertical axis is linear up to 1 ps and logarithmic afterwards.

References

(1) Nishitani, J.; Yamamoto, Y.-i.; West, C. W.; Karashima, S.; Suzuki, T. Binding Energy of Solvated Electrons and Retrieval of True UV Photoelectron Spectra of Liquids. *Sci. Adv.* **2019**, *5*, eaaw6896

(2) Schmidt, K. H.; Han, P.; Bartels, D. M. Radiolytic Yields of the Hydrated Electron from Transient Conductivity - Improved Calculation of the Hydrated Electron-Diffusion Coefficient and Analysis of Some Diffusion-Limited e^-(aq) Reaction-Rates. *J. Phys. Chem.* **1995**, *99*, 10530-10539.

(3) Koneshan, S.; Rasaiah, J. C.; Lynden-Bell, R. M.; Lee, S. H. Solvent Structure, Dynamics, and Ion Mobility in Aqueous Solutions at 25 Degrees C. *J. Phys. Chem. B* **1998**, *102*, 4193-4204.

(4) Jaygerin, J. P.; Ferradini, C. Compilation of Some Physicochemical Properties of Solvated Electrons in Polar Liquids. *J. Chim. Phys. Pcb* **1994**, *91*, 173-187.

(5) Xiang, H. W.; Laesecke, A.; Huber, M. L. A New Reference Correlation for the Viscosity of Methanol. *J. Phys. Chem. Ref. Data* **2006**, *35*, 1597-1620.

(6) Goncalves, F. A. M. M.; Trindade, A. R.; Costa, C. S. M. F.; Bernardo, J. C. S.; Johnson, I.; Fonseca, I. M. A.; Ferreira, A. G. M. Pvt, Viscosity, and Surface Tension of Ethanol: New Measurements and Literature Data Evaluation. *J. Chem. Thermodyn.* **2010**, *42*, 1039-1049.

(7) Iglev, H.; Trifonov, A.; Thaller, A.; Buchvarov, I.; Fiebig, T.; Laubereau, A. Photoionization Dynamics of an Aqueous Iodide Solution: The Temperature Dependence. *Chem. Phys. Lett.* **2005**, *403*, 198-204.

(8) Schmidt, K. H.; Han, P.; Bartels, D. M. Temperature-Dependence of Solvated Electron-Diffusion in H_2O and D_2O. *J. Phys. Chem.* **1992**, *96*, 199-206.

(9) Vilchiz, V. H.; Chen, X. Y.; Kloepfer, J. A.; Bradforth, S. E. Solvent Effects on Geminate Recombination Dynamics after Photodetachment. *Radiat. Phys. Chem.* **2005**, *72*, 159-167.